LANGMUIR

Article

pubs.acs.org/Langmuir

Kinetics of the Change in Droplet Size during Nanoemulsion Formation

Ankur Gupta, Vivek Narsimhan, T. Alan Hatton, and Patrick S. Doyle*

Department of Chemical Engineering, Massachusetts Institute of Technology, Cambridge, Massachusetts 02139, United States

Supporting Information

ABSTRACT: The evolution of droplet size during nanoemulsion formation is critical for the rational design of nanoemulsions in areas such as drug delivery and materials synthesis. In this article, we discuss the relative importance of various time scales involved in nanoemulsion formation and propose a population balance model for droplet breakup that takes into account the droplet's internal viscosity. The proposed model gives a qualitative agreement between average droplet size and polydispersity data for nanoemulsions prepared by high-pressure homogenization and ultrasonication. On the basis of these modeling results, we propose a correlation to obtain a parity plot for the droplet size data. We show that our model and correlation also work well with data from the existing literature. The proposed model and correlation can be used to guide future population balance studies and experimental preparation of nanoemulsions.

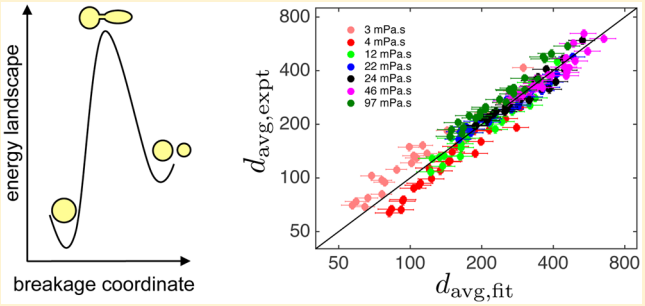

INTRODUCTION

Nanoemulsions are liquid−liquid dispersions with droplet sizes on the order of 100 nm. Because of their exceptional properties such as a large surface area and robust stability,[1−4] oil-in-water nanoemulsions are commonly used in drug delivery research to administer hydrophobic drugs,[5−8] development of healthy food drinks with hydrophobic nutrients,[9−11] nanoparticle and material synthesis,[12−15] and pharmaceutical crystallization.[16] A rational design of nanoemulsions for the aforementioned applications requires an understanding of the kinetics of the change in droplet size during nanoemulsion formation.

Nanoemulsions are prepared with three components—oil, water, and an emulsifier—through techniques such as high-pressure homogenization (HPH) or ultrasonication. During HPH, a macroemulsion is pushed through a narrow gap where droplets break under extreme shear conditions (Figure 1a).[1,2,17−22] Typically, the mixture is passed through the homogenizer multiple times until the droplet size becomes constant.[1,2,17−22] In an ultrasonicator, acoustic waves create cavitation bubbles that then implode, again generating sufficiently high shear conditions to break the droplets into smaller ones (Figure 1b).[1,21,23] As with HPH, ultrasonication is continued until the droplet size becomes independent of ultrasonication time.[24−26]

Several studies have reported that the average droplet size of a nanoemulsion decays exponentially with the number of passes in the homogenizer[2,18−22,27] and with ultrasonication time in the ultrasonicator.[21,24−26] The analysis of droplet size kinetics in the literature can be divided into two approaches. The first relates droplet size to the total energy input (or energy input density),[24−29] given by the product of power input and the number of passes or the ultrasonication time. Thus, the kinetics of nanoemulsion formation are absorbed in the calculation of total energy input. Though this approach is simple and intuitive, it does not provide any quantitative estimate of the dominant time scales. Moreover, reports show that there are parameters other than energy input that dictate droplet size

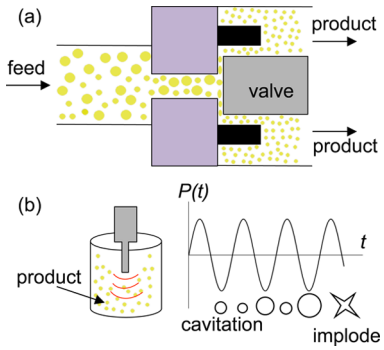

Figure 1. Schematic of methods for making nanoemulsions. (a) In a high-pressure homogenizer, the feed consists of a mixture of the oil and water phases and an emulsifier. When the feed passes through a narrow region inside the homogenizer, droplets break up because of high levels of shear and elongational stresses. (b) In an ultrasonicator, acoustic waves create pressure variations inside the continuous phase, leading to formation of cavitation bubbles. When the bubbles implode, they induce high-shear conditions and droplets break into smaller droplets.

Received: May 17, 2016
Revised: October 8, 2016
Published: October 11, 2016

DOI: 10.1021/acs.langmuir.6b01862
Langmuir 2016, 32, 11551−11559

(see the Supporting Information for an example).[18,20−22,24−27] The second approach utilizes population balance modeling for submicrometer emulsions.[30,31] However, as we show in this article, current literature studies incorrectly extrapolate the physics of macroemulsions (droplet size on the order of 100 μm) to the submicrometer range.[21]

An ability to predict steady state droplet size is also essential to understanding the kinetics of droplet size evolution. Several studies in the nanoemulsion literature[2,7,18,20,22] use the classical theory of Taylor[32,33] for an isolated droplet under laminar shear flow to predict the steady state droplet size. In his work, Taylor argued that for droplet breakup to occur, sufficient shear stress is required to overcome the interfacial stress. On the other hand, Hinze's correlation,[34] also used in several nanoemulsion studies,[25,27,29,35,36] was developed for turbulent flow and suggests that for droplet breakup to occur, sufficient inertial stress is required to overcome the interfacial stress holding the droplet together. Both Taylor and Hinze's correlations predict a droplet size that is independent of the disperse phase viscosity (i.e., the viscosity of the droplet's interior). This trend does not hold for nanoemulsions,[21] and we showed that another dimensionless group, the Ohnesorge number, Oh, is needed to describe the effect of the droplet's viscosity on its steady state size.

Here, we build upon our previous work and highlight the importance of incorporating the Ohnesorge number into the prediction of the droplet size evolution of nanoemulsions. We propose a new model for the droplet breakup frequency for incorporation into the population balance model to capture the effect of droplet viscosity, which has not been included in current models. We obtain qualitative agreement for average droplet size and polydispersity evolution with extensive experimental data of nanoemulsions obtained from HPH and ultrasonication. On the basis of these population balance modeling results, we propose a modified correlation for predicting droplet size over a wide range of experimental conditions. We anticipate that the proposed droplet breakup model and correlation will be useful for guiding future population balance studies and the experimental preparation of nanoemulsions.

MATERIALS AND METHODS

Materials. Hexadecane, silicone oils, mineral oil, and sodium dodecyl sulfate (SDS) were from Sigma-Aldrich.

Interfacial Tension Measurement. The pendant drop method was used to measure interfacial tension (Ramé-Hart goniometer) where an inverted oil drop with a volume of approximately 30−50 μL was created in a 5 wt % aqueous surfactant solution. The experiments were repeated five times, and a maximal error of ±1 mN/m was observed. The experiments were performed at 25 °C.

Rheology Measurement. The shear viscosity of various dispersed phases was measured using a cone and plate rheometer (60 mm diameter, 2° angle, AR-G2 TA Instruments) with a shear rate range of 1−500 s^{-1}. Newtonian behavior was observed for all oil phases in the given shear rate range. A maximal error of ±0.2 mPa s was observed in the viscosity measurements. The experiments were performed at 25 °C.

Nanoemulsion Synthesis. Nanoemulsions were prepared using high-pressure homogenization and ultrasonication. The first step in the synthesis involved mixing 1% oil (by volume) with a 175 mM SDS aqueous solution using a magnetic stir bar for 30 min at 700 rpm. For homogenization, 30 mL of the mixture was homogenized in an Avestin C-3 homogenizer (constant flow rate of 3 L/h) with four different pressure drops (ΔP = 35, 70, 105, and 140 bar) and 20 passes each; 50 μL samples were taken at regular intervals for dynamic light scattering (DLS) measurements. To keep the temperature of the nanoemulsions at room temperature (i.e., 25 °C), we allowed the sample to cool between subsequent passes. For ultrasonication, 2 mL mixtures were placed in plastic vials and ultrasonicated at three different ultrasonication amplitudes (20, 30, and 40%); 50 μL samples were removed at regular intervals for DLS measurements. A horn with a 24 mm diameter (Cole Parmer catalog no. EW-04710-38) at a frequency of 20 kHz was used for ultrasonication. To control the temperature during nanoemulsion formation, ultrasonication was performed in a water bath maintained at 25 °C.

Measurement of Nanoemulsion Droplet Size. Droplet size was monitored using dynamic light scattering (DLS). Each droplet size was obtained from a separate measurement on a 50 μL sample from the bulk nanoemulsion solution diluted in 500 μL of deionized water. The diluted sample was immediately subjected to dynamic light scattering (Wyatt Nanostar, 10 acquisitions of 5 s each). Three independent measurements were taken for each data point to gain confidence in the measurement. d_{avg} and polydispersity were extracted from raw DLS data using second-order cumulant analysis. We observed maximal errors of ±5% for d_{avg} and ±10% for polydispersity. Because droplet size measurements were performed immediately after nanoemulsions had been made, Ostwald ripening effects can be neglected. Also, the surfactant concentration in DLS samples exceeded the critical micelle concentration (CMC) and was sufficient to maintain nanoemulsion stability.

BACKGROUND AND THEORY

To design homogenization and ultrasonication processes effectively, it is important to understand the kinetics of droplet breakup from ∼100 μm to ∼100 nm in diameter.[20] In Figure 2,

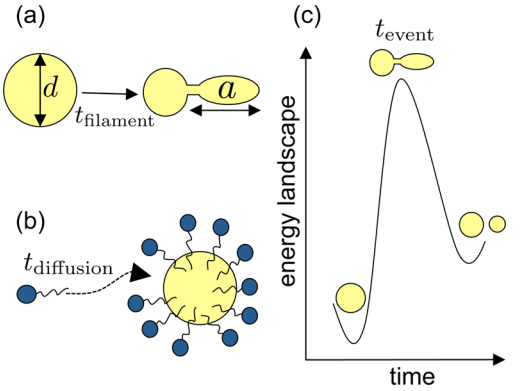

Figure 2. Overview of the different time scales in the droplet breakup process. (a) Before a droplet breaks, a filament is extruded from the parent droplet. For nanoemulsions, the length of the filament scales as $a \sim d\mathrm{Re}_d^{-0.5}$. The time scale of filament breakup is $t_{filament} \sim d/(u_d\mathrm{Re}_d)$. (b) When a new droplet is created, the surfactant molecules diffuse through the continuous phase and reach the surface of the droplet. The time scale of diffusion can be estimated by $t_{diffusion} \sim d^2 D_{diffusion}^{-1}$. (c) Similar to the case for a chemical reaction, there is a probability associated with a droplet breakup event. For nanoemulsions, the transition state depends on $\mathrm{We}_{eff} = \mathrm{We}\ \mathrm{Oh}^{-0.4}$.

we provide an overview of the various time scales involved in droplet breakup during the preparation of nanoemulsions. Three time scales are discussed in this section: the time scale of filament breakup ($t_{filament}$), the time scale of surfactant diffusion ($t_{diffusion}$), and the time scale for a successful droplet breakup event (t_{event}).

Before examining the various time scales, we briefly discuss our previous work to predict steady state droplet size d_∞.[21] Several studies in the nanoemulsion literature[2,7,18,20,22] use the

DOI: 10.1021/acs.langmuir.6b01862
Langmuir 2016, 32, 11551−11559

classical work of Taylor[32,33] to predict droplet size through the equation

$$\mathrm{Ca} = \frac{\mu_c \dot{\gamma} d_\infty}{\sigma} = B_1 \tag{1}$$

where Ca is the capillary number, μ_c is the continuous phase viscosity, $\dot{\gamma}$ is the shear rate in the continuous phase deforming the droplet, σ is the interfacial tension, and B_1 is a constant. Equation 1 is very intuitive because it implies that the droplet would not break if the applied stress $\tau_{applied} \sim \mu_c\dot{\gamma}$ is smaller than the stress σ/d holding the droplet together (i.e., the Laplace pressure). However, Taylor's theory cannot be applied to nanoemulsion synthesis because the theory assumes a laminar flow field whereas the flow inside a homogenizer and an ultrasonicator is turbulent.[17,21,23] Therefore, several studies of nanoemulsions[25,27,29,35,36] use the theory developed by Hinze,[34] who proposed that when a droplet of diameter d, viscosity μ_d, and density ρ_d is deformed by the outer phase with a stress $\tau_{applied}$, there will be two independent dimensionless groups for this system:

$$\mathrm{We} = \frac{\tau_{applied} d}{\sigma} \tag{2}$$

$$\mathrm{Oh} = \frac{\mu_d}{\sqrt{\rho_d \sigma d}} \tag{3}$$

where We (Weber number) is the ratio of the applied stress to the interfacial stress and Oh (Ohnesorge number) is the ratio of the viscocapillary time scale to the Rayleigh breakup time scale. A large We signifies that the applied stress dominates over the interfacial stress, and a large Oh means that the local viscous stresses dominate the inertial stresses for the droplet breakup dynamics. Oh is related to the Reynolds number of the droplet through the relation $\mathrm{Oh} = \mathrm{We}^{0.5}\mathrm{Re}_d^{-1}$ (the Reynolds number of the droplet is given by $\mathrm{Re}_d = (\rho_d u_d d)/\mu_d$, where $u_d \sim (\tau_{applied}/\rho_d)^{1/2}$. In his classical work, Hinze[34] proposed that when Oh ≪ 1 (i.e., $d \sim 100$ μm or macroemulsions), the final diameter size can be predicted by the following correlation:

$$\mathrm{We}_\infty = \frac{\tau_{applied} d_\infty}{\sigma} = B_2 \tag{4}$$

where d_∞ is the final droplet size and B_2 is a constant. Like Taylor,[32] Hinze also proposed that the dispersed phase continues to break down until the applied stress ($\tau_{applied}$) on the droplet balances the interfacial stress (σ/d). Hinze states that $\tau_{applied} \sim \rho_d u_d^2 \sim \rho_c(\varepsilon d_\infty)^{2/3}$, where the expression for the inertial stress is given by Kolmogorov's turbulent theory (u_d is the velocity scale inside the droplet, ρ_c is the continuous phase density, and ε is the input power density).[34] However, Hinze's theory assumes that Oh ≪ 1, an assumption that fails for nanoemulsions with a d of ∼100 nm (eq 3).

To account for the scenario in which Oh ≫ 1, we assume a binary fission process in which a filament extrudes from the parent droplet prior to droplet breakup (Figure 2a). We proposed in our previous work that the condition for droplet breakup should be given as follows:

$$\mathrm{We}_a = \frac{\rho_d u_a^2 a}{\sigma} = B_3 \tag{5}$$

where We_a is the Weber number based on the extruding filament, u_a is the velocity scale inside the filament, a is the length scale of the filament, and B_3 is a constant. Equation 5 assumes that the critical quantity is the Weber number based on the extruding filament instead of the Weber number based on the parent droplet. We showed that when Oh ≪ 1, or when the effect of droplet viscosity is negligible, the length scale and velocity scale of the filament are given as $a \sim d$ and $u_a \sim u_d$, respectively.[21] Thus, eq 5 is reduced back to Hinze's theory for Oh ≪ 1. However, for Oh ≫ 1, or when the effect of droplet viscosity is significant (the case relevant for nanoemulsions), $a \sim d\mathrm{Re}_d^{-0.5}$, and $u_a \sim u_d\mathrm{Re}_d^{0.5}$. Thus, after rearranging eq 5, we obtain the correlation for the final droplet size for Oh ≫ 1:[21]

$$\mathrm{We}_\infty \mathrm{Oh}_\infty^{-0.4} = \frac{\tau_{applied} d_\infty}{\sigma}\left(\frac{\mu_d}{\sqrt{\rho_d \sigma d_\infty}}\right)^{-0.4} = C_1 \tag{6}$$

where C_1 is a constant. Equation 6 indicates that there an effective Weber number $\mathrm{We}_{eff} = \mathrm{We}\ \mathrm{Oh}^{-0.4}$ exists and that droplet viscosity plays an important role in determining the final nanoemulsion droplet size. An estimate of $\tau_{applied}$ is needed to complete the prediction for d_∞. As $d \sim 100$ nm for nanoemulsions, the droplets are smaller than the Kolmogorov length scale $\lambda \sim [\mu_c^3/(\rho_c^3\varepsilon)]^{1/4} \sim 300$ nm (assuming $\mu_c = 10^{-3}$ Pa s, $\rho_c = 10^3$ kg/m^3, and $\varepsilon = 10^8$ W/kg).[37−39] In other words, even though the flow is turbulent at macroscopic length scales, it is viscous around the nanoemulsion droplet. In this viscous−turbulent regime, the applied stress on the droplet is given by the stress inside the smallest eddy $\tau_{applied} \sim (\mu_c\rho_c\varepsilon)^{1/2}$.[21,37−39] We can calculate the final droplet size d_∞ using the relations mentioned above. On the basis of this mechanism, we now discuss the various time scales of droplet breakup.

The time scale of filament breakup can be calculated via $t_{filament} \sim a/u_a \sim d/(u_d\mathrm{Re}_d)$ (because $a \sim d\mathrm{Re}_d^{-0.5}$ and $u_a \sim u_d\mathrm{Re}_d^{0.5}$). If we assume $\varepsilon \sim 10^8$ W/kg, $\mu_c \sim 10^{-3}$ Pa s, $\rho_c \sim 10^3$ kg/m^3, $\rho_d \sim 10^3$ kg/m^3, $\mu_d \sim 10^{-3}$ to 10^{-1} Pa s, and $u_d \sim (\tau_{applied}/\rho_d)^{1/2} \sim 1$ m/s,[21,34] we obtain $t_{filament} \sim 10^{-6}$ to 10^{-4} s. In several studies, however, it has been observed that it takes several passes in a HPH (residence time of ∼1 s) and several minutes in an ultrasonicator to make nanoemulsions.[21,24−26] Therefore, the filament breakup time scale is several orders of magnitude shorter than the time scale of nanoemulsion formation.

When new droplets are created, surfactant molecules diffuse through the continuous phase to reach the surface of the new droplets (Figure 2b). The relevant length scale of surfactant diffusion is the diameter of the droplet (d) as nanoemulsions are prepared in an environment where surfactant is in excess. The time scale of surfactant diffusion can be calculated using $t_{diffusion} \sim d^2/D_{surfactant}$, where $D_{surfactant}$ is the diffusivity of the surfactant in the continuous phase, assuming $d \sim 100$ nm, $D_{surfactant} \sim 10^{-9}$ m^2/s, and $t_{diffusion} \sim 10^{-5}$ s. The rate of this process is also very fast compared to the rate observed during nanoemulsion preparation.

In some literature studies, it is argued that the kinetics of droplet size change is related to the dynamics of interfacial tension changes.[29] Though dynamic interfacial tension can play a role in dictating the droplet size of nanoemulsions, the change in interfacial tension is not large enough to explain the variations observed during the preparation of nanoemulsions. For instance, Donsi et al.[29] report a maximal change in interfacial tension of ∼20% for a wide range of surfactants. Hence, if the dynamics of interfacial tension were dominating the kinetics of droplet size change, the average droplet size

DOI: 10.1021/acs.langmuir.6b01862
Langmuir 2016, 32, 11551−11559

should change at most by ∼12% (see eq 6). In reality, the droplet size is reduced by almost 80% with an increase in the homogenizer number of passes or the ultrasonication time.[20−22,24] Therefore, the surfactant dynamics do not dominate the kinetics of change in droplet size and make only a minor contribution.

The time scale associated with the probability of a successful droplet breakup event (t_{event}) is widely used in population balance modeling studies.[30,31,40−42] The approach proposes that drops undergo a transition from an initial state (large droplet) to a final state (small droplet), with the path between these states dominated by an energy barrier (Figure 2c). For a successful droplet breakup to occur, the kinetic energy of droplet deformation should overcome the increase in interfacial energy.[43] Thus, the frequency of a successful droplet breakup is

$$\nu_{event} \sim \frac{1}{t_{event}} \sim \frac{1}{t_{eddy}} \exp\left(-\frac{E_I}{E_K}\right) \tag{7}$$

where ν_{event} is the frequency of a successful droplet breakup event, t_{event} is the time scale of a successful droplet breakup event, t_{eddy} is the eddy time scale, E_I is the interfacial energy of the droplet, and E_K is the kinetic energy of the droplet. The value of t_{eddy} is taken as the maximum of the Kolomogorov time scale $t_{Kolmogorov} = [\mu_c/(\rho_c\varepsilon)]^{1/2}$ and droplet eddy time scale $t_{d,eddy} = (d_2/\varepsilon)^{1/3}$. In other words, t_{eddy} would be taken as $t_{Kolmogorov}$ when the droplet size is smaller than the Kolmogorov length scale and as $t_{d,eddy}$ otherwise. The prefactor in eq 7 is a measure of eddy breakup frequency, and the exponential describes the probability of a successful droplet breakup event. Energies E_I and E_K scale as

$$E_I \sim \sigma d^2 \tag{8}$$

$$E_K \sim \tau_{applied} d^3 \tag{9}$$

Combining eqs 7−9, we obtain

$$\nu_{event} = \frac{1}{t_{event}} = \frac{K_1}{t_{eddy}} \exp\left(-K_2 \frac{\sigma}{\tau_{applied} d}\right) = \frac{K_1}{t_{eddy}} \exp\left(-K_2 \frac{1}{We}\right) \tag{10}$$

where K_1 and K_2 are constants on the order of unity. As the frequency of droplet breakup (ν_{event}) depends on the diameter of the droplet, there is a range of breakup frequencies that operate during the emulsification process. With the reduction in average droplet size, the frequency becomes smaller and the rate of change of droplet size becomes slower. At long times when $d \sim d_\infty$, the rate of change in droplet size becomes negligible. Equation 7 is consistent with Hinze's theory[34] that $d \to d_\infty$ when We = C_1 (eq 4). However, as Oh ≫ 1 for nanoemulsions, d_∞ should be a strong function of droplet viscosity (μ_d). This is not captured by eq 10. Further, as we show in Results and Discussion, the values of t_{event} as predicted by eq 10 are less realistic than those given by our proposed model.

We propose that the transition state barrier for droplet breakup is related to the filament extrusion process (Figure 2c), and E_I and E_K should be calculated as the interfacial energy ($E_I \sim \sigma a^2$) and kinetic energy ($E_K \sim \rho_d u_a^2 a^3$) of the extruding filament. For macroemulsions, because $a \sim d$ and $u_a \sim u_d$,[21] E_I and E_K of the extruding filament are the same as those for the parent droplet. However, for nanoemulsions, because $a \sim d\mathrm{Re}_d^{-0.5}$ and $u_a \sim u_d\mathrm{Re}_d^{0.5}$, E_I and E_K are[21]

$$E_I \sim \sigma a^2 \sim \sigma d^2 \mathrm{Re}_d^{-1} \tag{11}$$

$$E_K \sim \rho_d u_a^2 a^3 \sim \tau_{applied} d^3 \mathrm{Re}_d^{-0.5} \tag{12}$$

Combining eqs 10−12, we obtain

$$\nu_{event} = \frac{1}{t_{event}} = \frac{K_1}{t_{eddy}} \exp\left(-K_2 \frac{\sigma \mathrm{Re}_d^{-0.5}}{\tau_{applied} d}\right) = \frac{K_1}{t_{eddy}} \exp\left(-K_2 \frac{1}{We_{eff}^{1.25}}\right) \tag{13}$$

where We_{eff} = We $Oh^{-0.4}$. Equation 13 is able to capture the effect of μ_d on droplet size, whereas eq 10 fails to do so.

We perform population balance modeling[44] to understand the evolution of the droplet size distribution and to compare the droplet breakup frequency relations described in eqs 10 and 13. We neglect droplet coalescence in our model because our experiments were performed at dilute oil volume fractions. The number density $n(d,t)$ of droplets for a given size d and at a given time t is

$$\frac{\partial n(d,t)}{\partial t} = \int_d^\infty \beta(d,x)\nu_{event}(x)n(x,t)\,dx - \nu_{event}(d)n(d,t) \tag{14}$$

where $\beta(d,x)$ is the daughter distribution function that gives the fraction of droplets with size x that break into droplets with size d and $\nu_{event}(d)$ is the breakage frequency of a droplet of size d (eqs 10 and 13). The integral term in eq 14, called the birth term, determines the number of droplets of size d created upon the breakup of larger droplets. The second, or death term, represents the number of droplets of size d that break into smaller droplets. For the daughter distribution function, we assume that equal volume droplets[41] are generated:

$$\beta(d,x) = 2\delta\left(d - \frac{x}{2^{1/3}}\right) \tag{15}$$

where $\delta(x)$ is the Dirac delta function. We solve for the distribution $n(d,t)$ by converting eqs 14 and 15 into a system of ODEs to obtain

$$\frac{dn_i}{dt} = 2\nu_{event}(x_j)n_j - \nu_{event}(x_i)n_i \tag{16}$$

where $n_i = n(x_i,t)\,dx_i$ represents the number of droplets between sizes x_i and $x_i + dx$ at a given time t and $x_j = 2^{1/3}x_i$. The equations were solved for 501 bins with the mean bin size given by a geometric progression series $x_i = 50 \times 10^{-6} \times 1.05^i$ (in m) where $i = [-250, 250]$. The values of physical properties were kept the same as in Table 1, and constants K_1 and K_2 for $\nu_{event}(d)$ were taken to be 0.1 and 0.6, respectively, for all the simulations.

RESULTS AND DISCUSSION

We prepared oil-in-water nanoemulsions with both a homogenizer and an ultrasonicator. The aim of these experiments was to observe the evolution of droplet size with the number of passes (N) in the homogenizer, and with the ultrasonication time (t_{us}) in the ultrasonicator. Dilute nanoemulsions with a composition of 1% (by volume) oil in

DOI: 10.1021/acs.langmuir.6b01862
Langmuir 2016, 32, 11551−11559

Table 1. Physical Properties of Oil Phases Used in Nanoemulsion Preparation[a]

oil	μ_d (mPa s)	ρ_d (kg/m^3)	σ (mN/m)
hexadecane	3 ± 0.2	764	4.9 ± 1.0
silicone oil	4 ± 0.2	914	7.6 ± 1.0
75:25 silicone mixture	12 ± 0.2	916	8.8 ± 1.0
50:50 silicone mixture	22 ± 0.2	928	9.0 ± 1.0
mineral	24 ± 0.2	840	7.4 ± 1.0
25:75 silicon mixture	46 ± 0.2	938	7.9 ± 1.0
viscous silicone oil	97 ± 0.2	958	8.7 ± 1.0

[a]The mixtures of silicone oils are based on volume percent.

aqueous solution of 175 mM sodium dodecyl sulfate (SDS) were prepared with four different pressure drops (ΔP) and 20 passes in the homogenizer. Nanoemulsions of the same composition were also prepared in an ultrasonicator for 20 min using three different amplitudes (A) at 20 kHz. The droplet size was monitored at regular intervals to capture the variation in droplet size with N and t_{us}. A low oil volume fraction was used to avoid coalescence and non-Newtonian effects, and SDS was used to avoid surfactant size effects.[36,45] The concentration of SDS was maintained at several times above its CMC to ensure that the surfactant was present in abundance in the continuous phase. Seven different oil phases were used to explore the effect of droplet viscosity on the evolution of nanoemulsion droplet size. The values of oil viscosity (μ_d) and interfacial tension of the oil phase with the aqueous surfactant solution (σ) are summarized in Table 1 (details of the experimental procedure are provided in Materials and Methods). The droplet size was measured by DLS.

The evolution of the droplet size for different oil viscosities (μ_d) is shown in Figure 3. The droplet size changes from approximately 400−700 to 100−300 nm. The average droplet size (d_{avg}) first decreases and then becomes roughly constant with an increasing N in the homogenizer, or with an increasing t_{us} in the ultrasonicator. The trend is consistent with literature reports, where droplet breakage dominates over droplet coalescence.[18,20,24,26] Also, the d_{avg} values were found to be comparable for the homogenizer and the ultrasonicator, as anticipated on the basis of the similar values of ε for the two methods[21] (eq 6). The final average droplet size depends strongly on μ_d, which is consistent with our prediction of the strong role played by Oh (eq 6). Though the final size depends on μ_d, the rate of droplet size decay appears to be independent of μ_d. Also, the evolution of polydispersity does not show any significant trend with μ_d. We compare this trend with population balance modeling results in subsequent paragraphs.

The dependence of droplet size on pressure drop ΔP and sonication amplitude A was discussed in our previous work[21] (see the Supporting Information for the experimental data). The final drop size decreases with an increasing pressure drop (ΔP) across the homogenizer because the power input ε increases as ΔP increases (eq 6).[21] In contrast, the steady state droplet size remains roughly constant with changes in amplitude (A) in the ultrasonicator as ε does not depend strongly on A.[21] Also, the rate of droplet size decay does not show a significant dependence on ΔP or A. We also compare these trends with population balance modeling results in subsequent paragraphs.

We solved eqs 10, 13, and 16 to understand the evolution of droplet size distribution during nanoemulsion formation. The values of physical properties listed in Table 1 were used for all simulations. To obtain the initial droplet size distribution, we analyzed several microscopic images of the homogenizer/ultrasonicator feed (see the Supporting Information for details). On the basis of our image analysis, the initial droplet size distribution was assumed to be a log-normal distribution with

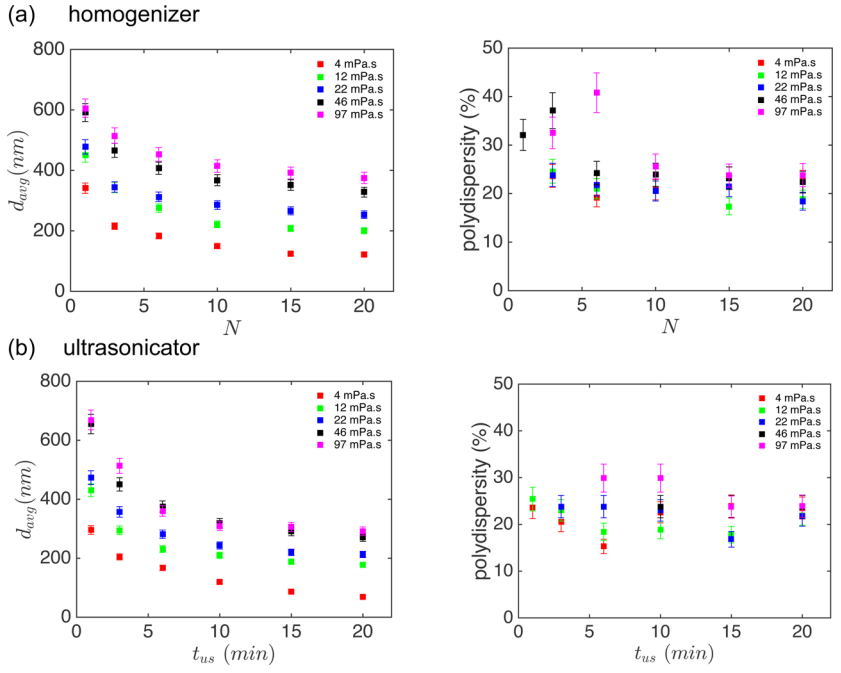

Figure 3. Experimental data for nanoemulsions with varying μ_d values. (a) d_{avg} and polydispersity data for nanoemulsions prepared by a homogenizer with a ΔP of 35 bar. (b) Droplet size and polydispersity data for nanoemulsions prepared by an ultrasonicator with an amplitude A of 20%. For both the homogenizer and ultrasonicator, the profiles for d_{avg} show that the final droplet size increases with an increase in μ_d and the rate of d_{avg} decay is roughly constant for different μ_d values. There is no significant trend of polydispersity with μ_d.

DOI: 10.1021/acs.langmuir.6b01862
Langmuir 2016, 32, 11551−11559

an average droplet size of 50 μm with 100% polydispersity, where polydispersity is defined as $\sqrt{\frac{\sum_i n_i d_i^2 / \sum_i n_i}{(\sum_i n_i d_i / \sum_i n_i)^2}} - 1$. Moreover, we observed that the final droplet size is insensitive to the choice of initial droplet size distribution (see the Supporting Information).

Figure 4 compares population balance results from eqs 10 and 13 for two different μ_d values. The value of ε was taken to be 3.4 × 10^7 W/kg, which corresponds to a ΔP of 35 bar in HPH (see ref 21 for details). Equation 13 predicts different profiles for d_{avg} depending on μ_d (consistent with experiments), whereas eq 10 fails to do so (Figure 4a). Also, eq 10 predicts a significantly faster reduction in droplet size (and is thus less realistic) because it does not include the effect of Oh, which becomes dominant when d_{avg} < 1 μm (eq 3). After a rapid reduction in droplet size until $d_{avg} \sim 1$ μm, d_{avg} profiles from eq 13 decay slowly because ν_{event} decreases sharply with further decreases in d_{avg}. Additionally, d_{avg} curves for different μ_d values become parallel after $t \sim 10^{-3}$ s because We_{eff} is the same for different viscosities at long times. When we compare the evolution of droplet size distribution from eq 13 for two different μ_d values, we observe that polydispersity first increases and then decreases (Figure 4b). This happens because the daughter distribution function forces an equal volume droplet breakup leading to an initial rise in polydispersity followed by a subsequent decay. After $t \sim 10^{-3}$ s, the polydispersity is roughly constant for both μ_d values (Figure 4b).

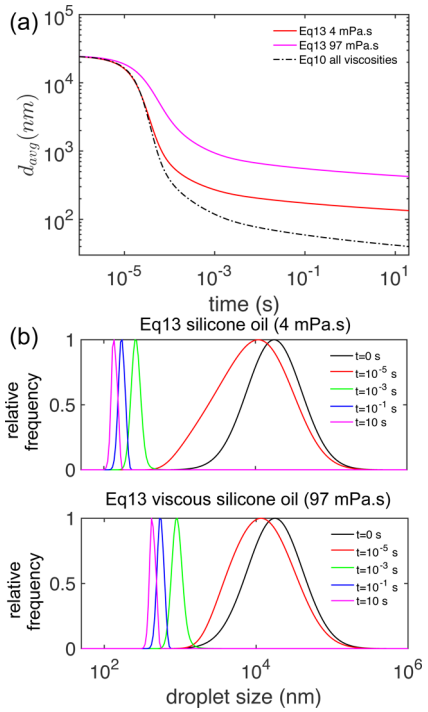

Figure 4. Overview of the population balance modeling results. (a) Comparison of the evolution of d_{avg} for two different μ_d values using eqs 10 and 13. Equation 13 predicts different d_{avg} profiles for different μ_d values, unlike eq 10. (b) Droplet size distribution at different time points determined using eq 13 for two different viscosities. The distributions are plotted by dividing n_i (eq 16) by $n_{i,max}$ so that the maximum value is always unity. The values of parameters K_1 = 0.1, K_2 = 0.6, and ε = 3.4 × 10^7 W/kg were used in all simulations. The physical properties of oils were kept the same as in Table 1.

Figure 5 compares d_{avg} and polydispersity data from HPH experiments with population balance modeling results for different μ_d values. A residence time of 1 s per homogenizer pass was assumed because the homogenzier volume is on the order of 10^{-6} m^3 and the homogenizer flow rate is ∼10^{-6} m^3 s^{-1}. The value of ε was taken to be 3.4 × 10^7 W/kg, which corresponds to a ΔP of 35 bar in HPH. Results from eq 13 agree qualitatively with the following trends from experiments: (a) different d_∞ for different μ_d and (b) parallel d_{avg} profiles (Figure 5a). On the other hand, results from eq 10 show no variation with μ_d (all curves are the same) and predicts a decrease in d_{avg} faster than that predicted by eq 13. Though eq 13 is an improvement over eq 10, our model significantly underpredicts the rate of droplet size decay for early passes N = 1−6. The disagreement could be attributed to the following factors. (a) Our model does not account for the flow field inhomogeneity within each homogenizer pass, a factor that will increase d_{avg} when compared to the value for a completely homogeneous environment. (b) We do not include temperature effects in our model that are likely to change the d_{avg} profiles because the model predictions are highly sensitive to physical properties. (c) The assumption of residence time being 1 s per homogenizer pass may be an overestimation leading to a higher disagreement for N = 1−6. A computational fluid dynamics model coupled with energy and population balances can incorporate these effects, which would be interesting to study in the future. Equations 10 and 13 predict that the polydispersity remains roughly constant and saturates at a value of 9−10% irrespective of μ_d (Figure 5b). The inhomogeneity in shear field around droplets leads to differently sized daughter

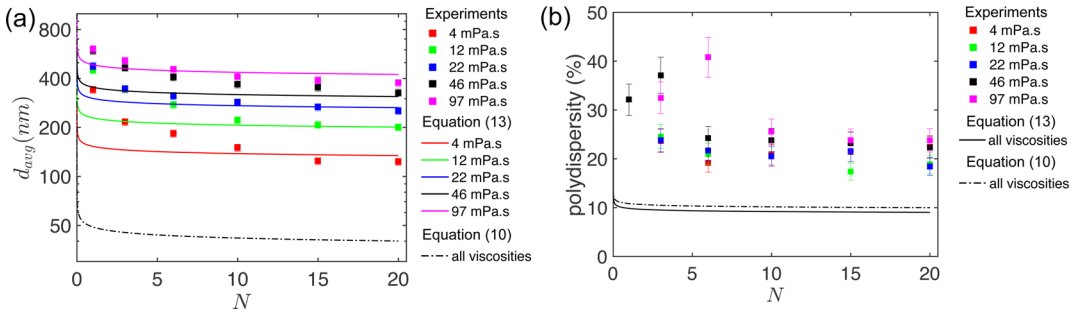

Figure 5. Comparison of d_{avg} profiles from experiments and population balance for different μ_d values. (a) Qualitative agreement between experiments and the model obtained for d_{avg} with eq 13, but not eq 10. (b) As in experiments, the polydispersity remains constant with N and μ_d using both eqs 10 and 13. However, both the models significantly underestimate the polydispersity. The values of parameters K_1 = 0.1, K_2 = 0.6, and ε = 3.4 × 10^7 W/kg were used in all simulations. The physical properties of oils were those listed in Table 1.

DOI: 10.1021/acs.langmuir.6b01862
Langmuir 2016, 32, 11551−11559

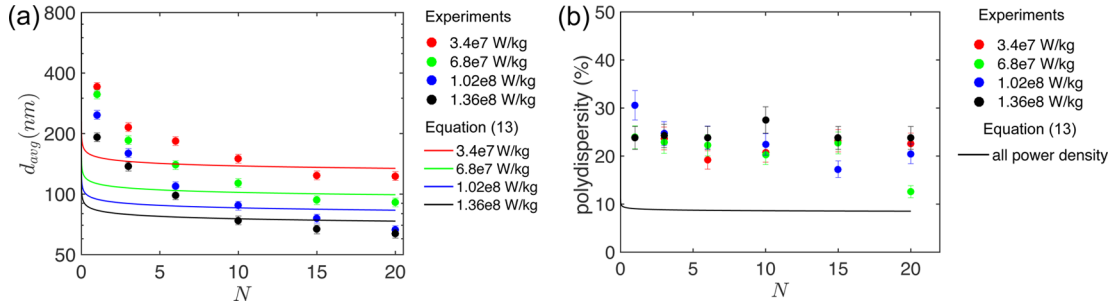

Figure 6. Comparison of experiments performed at different ε values with results from population balance modeling using eq 13. Silicone oil with a viscosity of 4 mPa s was used for the following comparison. Qualitative agreement between the experiments and the model is obtained for d_{avg}. (b) As in experiments, the polydispersity from the model remains constant with N and ε. However, the model significantly underestimates the polydispersity. The values of parameters $K_1 = 0.1$, $K_2 = 0.6$, and $\mu_d = 4$ mPa s were used in all simulations. The physical properties of oils were those listed in Table 1.

drops, and recent studies of large emulsion droplets suggest that several factors such as droplet viscosity, power density, and interfacial tension dictate the daughter distribution function.[46] We have ignored such complications in our current model, which could be the reason for the discrepancies between model predictions and experiments.

Figure 6 compares d_{avg} and polydispersity data from experiments with population balance modeling for different ε values. Silicone oil with a viscosity of 4 mPa s was used for the following comparison. We obtain qualitatively similar results from eq 13 and experiments, as $d_{avg,\infty}$ decreases with an increase in ε and the d_{avg} profiles appear to be parallel. The variation of t_{event} with ε involves two competing factors in our model: an increase in the $1/t_{eddy}$ term and a decrease in the efficiency term with an increase in ε. Because we ignore the flow field inhomogeneity in the model, we significantly underpredict changes in d_{avg} for $N = 1-6$. Also, an increase in ε increases the local heating effects in experiments, a factor currently ignored in our model. Similar to the trends with μ_d, polydispersity is insensitive to ε as polydispersity is set by the daughter distribution function. We believe that to investigate the effect of ε in detail, future studies should allow for changes in ε within the same d_{avg} profile. For instance, nanoemulsions can be homogenized with $\Delta P = 300$ bar for the first 10 passes and with $\Delta P = 3000$ bar for 10 additional passes.

In our population balance model, the frequency of droplet breakup ν_{event} decays slowly at long times and hence is nearly constant. Assuming ν_{event} is constant, solution of the first two moments of the droplet size distribution from eq 14 yields an exponential decay expression for average droplet size. Thus, several prior researchers have used an exponential decay in droplet size to analyze the kinetics of droplet size data.[1,2,20−22] However, none of the aforementioned studies estimated $d_{avg,\infty}$ but instead used it as a purely fitting parameter. Moreover, the prior studies did not provide a rationale for the variation of decay rate with physical properties. Therefore, we propose a correlation for d_{avg} by combining the expression for steady state droplet size ($d_{avg,\infty}$) from eq 6 with a single-exponential decay:

$$d_{avg,fit}(N) = C_1 \frac{\sigma^{5/6}\mu_d^{1/3}}{(\rho_d\sigma)^{1/6}(\mu_c\rho_c\varepsilon)^{5/12}} + C_2 \exp\left(-\frac{N}{N_b}\right) \quad (17)$$

where C_1, C_2, and N_b are constants. We can assume N_b to be a constant because Figures 5 and 6 show that the d_{avg} decay rate is not sensitive to ε or μ_d. By using the physical properties listed in Table 1, we evaluate $d_{avg,fit}$ from eq 17 for different values of N, μ_d, and ε with C_1, C_2, and N_b as parameters. We maximized the following least-squares sum to obtain the values of C_1, C_2, and N_b:

$$R^2 = 1 - \frac{\sum_\varepsilon \sum_{\mu_d} \sum_N (d_{avg,fit} - d_{avg,expt})^2}{\sum_\varepsilon \sum_{\mu_d} \sum_N d_{avg,expt}^2} \quad (18)$$

The maximal R^2 value of 0.985 occurs at $C_1 = 0.10$, $C_2 = 271$ nm, and $N_b = 3.2$. The C_1 value of 0.10 is slightly different from that obtained in our previous work[21] (i.e., 0.057) because we fit the droplet size data for all values of N, and not just $N = 20$. C_1 is a measure of the length of filament extrusion during droplet breakup (see discussion of Figure 2a). The N_b value of 3.2 is consistent with our experimental data, where $d_{avg,expt}$ remains roughly constant after $N = 10$. By using the optimal values of C_1, C_2, and N_b, we show the variation of droplet size from experiments ($d_{avg,expt}$) with droplet size from correlation ($d_{avg,fit}$) in Figure 7. Here, each data point in the parity plot represents

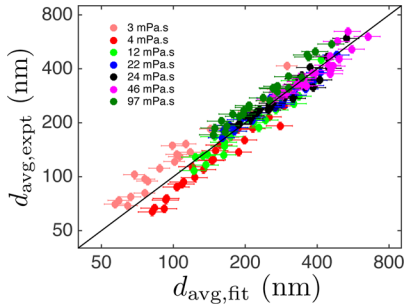

Figure 7. Parity plot using eq 17 obtained for kinetic droplet size data prepared with different values of μ_d, ε, and N. We obtain very good agreement between $d_{avg,fit}$ and $d_{avg,expt}$ using $C_1 = 0.10$, $C_2 = 271$ nm, and $N_b = 3.2$.

one independent experiment for a set of N, μ_d, and ε. Thus, we are able to estimate the evolution of droplet size over a wide range of operating conditions by combining steady state droplet size and single-exponential decay. We note that the deviation of $d_{avg,fit}$ from $d_{avg,expt}$ is higher for lower values of μ_d because our assumption of Oh $\gg$ 1 is less valid than for higher values of μ_d.[21] Lastly, a similar curve can be obtained for ultrasonication data (see the Supporting Information).

To show that our model and correlation are universal in nature, we compare the results from our model and correlation with an existing data set from the literature. We used the d_{avg}

DOI: 10.1021/acs.langmuir.6b01862
Langmuir 2016, 32, 11551−11559

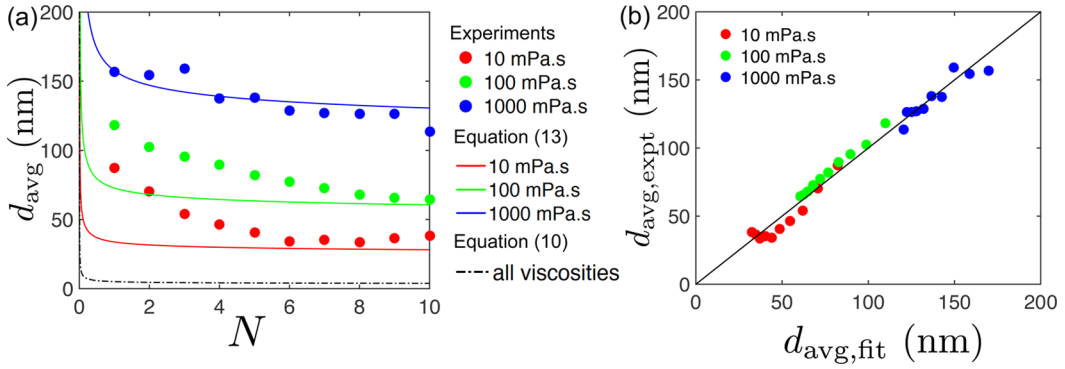

Figure 8. Comparison of (a) our model (eq 13) and (b) correlation (eq 17) with existing data from the literature.[22] We obtain a clear improvement in agreement from eq 13 when compared to that with eq 10 because our model can capture the effect of μ_d. Also, our correlation shows very good agreement for three different oil viscosities. The experimental data were taken from ref 22. The values of σ = 10 mN/m, $\rho_c = 10^3$ kg/m^3, μ_c = 1 mPa s, $\rho_d = 10^3$ kg/m^3, and $\varepsilon = 10^9$ W/kg were used for all the oils. The population balance calculations were performed using $K_1 = 10^{-4}$ and K_2 = 0.15. The correlation was obtained using C_1 = 0.04, C_2 = 71 nm, and N_b = 4.7.

data for different homogenizer passes and μ_d from Meleson et al.[22] to compare with our model (eq 13) and correlation (eq 17). Figure 8 provides an overview of the comparison among the model, correlation, and data from the literature. Because we do not know the exact physical properties of the nanoemulsion system, representative values of σ = 10 mN/m, $\rho_c = 10^3$ kg/m^3, μ_c = 1 mPa s, $\rho_d = 10^3$ kg/m^3, and $\varepsilon = 10^9$ W/kg were used for the three different nanoemulsion systems. The population balance calculations were performed using $K_1 = 10^{-4}$ and K_2 = 0.15. The correlation was obtained using C_1 = 0.04, C_2 = 71 nm, and N_b = 4.7. Our model yields qualitatively similar profiles for all three oil viscosities (Figure 8a), whereas the existing model fails to capture the effect of oil viscosity. The possible reasons for disagreement between experimental data and our model have been detailed in the discussion of Figure 5. Finally, we show that the proposed correlation works very well for the existing data in the literature (Figure 8b) and can capture the effect of dispersed phase viscosity. This result underscores the importance of including the Ohnesorge number as a parameter when modeling the kinetics of nanoemulsion formation.

CONCLUSION

A number of studies of the preparation of nanoemulsions have addressed the effects of process variables on final nanoemulsion droplet size, and on the kinetics of droplet size evolution, through the extrapolation of theories for macroemulsions to the nanoemulsion domain. These approaches do not take into account the impact of internal phase physical properties on final droplet size, however, specifically that of the internal phase viscosity. In addition, no allowances are made for the fact that the final droplets are smaller than the Kolmogorov eddy length scale and are therefore subjected to shear conditions in the viscous−turbulent regime. We have proposed a new droplet breakup frequency model for use in population balance analyses of droplet dynamics to account for these effects and overcome these earlier limitations in the presented models. In our case, the model breakup frequency is shown to be dependent on an effective Weber number $We_{eff} = We\ Oh^{-0.4}$, which captures the effect of the dispersed phase viscosity on the droplet breakup kinetics and on the final steady state droplet size. Good qualitative agreement between the model and experimental data in their dependence on parameters such as droplet viscosity and power density is obtained and provides a rationale for the development of a correlation for the effective prediction of the exponential decay in droplet size during either homogenization or ultrasonication.

Further enhancements to the experimental studies and modeling of nanoemulsion preparation processes should allow for incorporation of the effects of interfacial tension and continuous phase viscosity in the predictive correlation derived in this work. Deeper insight into nanoemulsion droplet evolution during processing could be gleaned through computational fluid dynamics simulations coupled with energy and population balances to incorporate the effects of flow field inhomogeneities and temperature changes due to viscous dissipation. The results of such investigations should allow for a rational scale-up of nanoemulsion synthesis for a wide range of applications, including drug delivery, food science, and materials synthesis, among others.

ASSOCIATED CONTENT

Supporting Information

The Supporting Information is available free of charge on the ACS Publications website at DOI: 10.1021/acs.langmuir.6b01862.

Details of choosing the initial droplet size distribution, droplet size data for different ε inputs, droplet size data plotted versus energy input, and parity plot for ultrasonicator data (PDF)

AUTHOR INFORMATION

Corresponding Author

*E-mail: pdoyle@mit.edu.

Notes

The authors declare no competing financial interest.

ACKNOWLEDGMENTS

The authors acknowledge Eni S.p.A for their financial support of this project. We also acknowledge the Biophysical Instrumentation Facility at the Massachusetts Institute of Technology where DLS measurements were performed (NSF-0070319).

REFERENCES

(1) Gupta, A.; Eral, H. B.; Hatton, T. A.; Doyle, P. S. Nanoemulsions: formation, properties and applications. *Soft Matter* **2016**, *12*, 2826−2841.

DOI: 10.1021/acs.langmuir.6b01862
Langmuir 2016, 32, 11551−11559

(2) Mason, T. G.; Wilking, J. N.; Meleson, K.; Chang, C. B.; Graves, S. M. Nanoemulsions: formation, structure, and physical properties. *J. Phys.: Condens. Matter* **2006**, *18*, R635−R666.
(3) Solans, C.; Izquierdo, P.; Nolla, J.; Azemar, N.; Garciacelma, M. Nano-emulsions. *Curr. Opin. Colloid Interface Sci.* **2005**, *10*, 102−110.
(4) Tadros, T.; Izquierdo, P.; Esquena, J.; Solans, C. Formation and stability of nano-emulsions. *Adv. Colloid Interface Sci.* **2004**, *108−109*, 303−318.
(5) Kumar, M.; Misra, A.; Babbar, A. K.; Mishra, A. K.; Mishra, P.; Pathak, K. Intranasal nanoemulsion based brain targeting drug delivery system of risperidone. *Int. J. Pharm.* **2008**, *358*, 285−91.
(6) Sarker, D. Engineering of Nanoemulsions for Drug Delivery. *Curr. Drug Delivery* **2005**, *2*, 297−310.
(7) Lovelyn, C. Current State of Nanoemulsions in Drug Delivery. *J. Biomater. Nanobiotechnol.* **2011**, *02*, 626−639.
(8) Shakeel, F.; Baboota, S.; Ahuja, A.; Ali, J.; Aqil, M.; Shafiq, S. Nanoemulsions as vehicles for transdermal delivery of aceclofenac. *AAPS PharmSciTech* **2007**, *8*, 191.
(9) McClements, D. J.; Rao, J. Food-Grade Nanoemulsions: Formulation, Fabrication, Properties, Performance, Biological Fate, and Potential Toxicity. *Crit. Rev. Food Sci. Nutr.* **2011**, *51*, 285.
(10) McClements, D. J. Edible nanoemulsions: fabrication, properties, and functional performance. *Soft Matter* **2011**, *7*, 2297−2316.
(11) Rao, J.; McClements, D. J. Food-grade microemulsions, nanoemulsions and emulsions: Fabrication from sucrose monopalmitate & lemon oil. *Food Hydrocolloids* **2011**, *25*, 1413−1423.
(12) Anton, N.; Benoit, J.-P.; Saulnier, P. Design and production of nanoparticles formulated from nano-emulsion templates-a review. *J. Controlled Release* **2008**, *128*, 185−99.
(13) Landfester, K. Miniemulsion polymerization and the structure of polymer and hybrid nanoparticles. *Angew. Chem., Int. Ed.* **2009**, *48*, 4488−507.
(14) Asua, J. M. Miniemulsion polymerization. *Prog. Polym. Sci.* **2002**, *27*, 1283−1346.
(15) Gu, T.; Yeap, E. W.; Somasundar, A.; Chen, R.; Hatton, T. A.; Khan, S. A. Droplet Microfluidics with a Nanoemulsion Continuous Phase. *Lab Chip* **2016**, *16*, 2694.
(16) Eral, H. B.; López-Mejías, V.; O'Mahony, M.; Trout, B. L.; Myerson, A. S.; Doyle, P. S. Biocompatible Alginate Microgel Particles as Heteronucleants and Encapsulating Vehicles for Hydrophilic and Hydrophobic Drugs. *Cryst. Growth Des.* **2014**, *14*, 2073−2082.
(17) Floury, J.; Bellettre, J.; Legrand, J.; Desrumaux, A. Analysis of a new type of high pressure homogeniser. A study of the flow pattern. *Chem. Eng. Sci.* **2004**, *59*, 843−853.
(18) Mason, T. G.; Graves, S. M.; Wilking, J. N.; Lin, M. Y. Extreme emulsification: formation and structure of nanoemulsions. *Condens. Matter Phys.* **2006**, *9*, 193−199.
(19) Wilking, J. N.; Mason, T. G. Irreversible shear-induced vitrification of droplets into elastic nanoemulsions by extreme rupturing. *Phys. Rev. E* **2007**, *75*, 041407.
(20) Helgeson, M. E.; Moran, S. E.; An, H. Z.; Doyle, P. S. Mesoporous organohydrogels from thermogelling photocrosslinkable nanoemulsions. *Nat. Mater.* **2012**, *11*, 344−352.
(21) Gupta, A.; Eral, H. B.; Hatton, T. A.; Doyle, P. S. Controlling and predicting droplet size of nanoemulsions: scaling relations with experimental validation. *Soft Matter* **2016**, *12*, 1452−1458.
(22) Meleson, K.; Graves, S.; Mason, T. G. Formation of concentrated nanoemulsions by extreme shear. *Soft Mater.* **2004**, *2*, 109−123.
(23) Mason, T. J.; Lorimer, J. P. *Applied Sonochemistry*; Wiley-VCH: New York, 2002.
(24) Delmas, T.; Piraux, H.; Couffin, A.-C.; Texier, I.; Vinet, F.; Poulin, P.; Cates, M. E.; Bibette, J. How to prepare and stabilize very small nanoemulsions. *Langmuir* **2011**, *27*, 1683−1692.
(25) Leong, T. S. H.; Wooster, T. J.; Kentish, S. E.; Ashokkumar, M. Minimising oil droplet size using ultrasonic emulsification. *Ultrason. Sonochem.* **2009**, *16*, 721−7.
(26) Tang, S. Y.; Shridharan, P.; Sivakumar, M. Impact of process parameters in the generation of novel aspirin nanoemulsions-comparative studies between ultrasound cavitation and microfluidizer. *Ultrason. Sonochem.* **2013**, *20*, 485−97.
(27) Gothsch, T.; Finke, J. H.; Beinert, S.; Lesche, C.; Schur, J.; Büttgenbach, S.; Müller-Goymann, C.; Kwade, a. Effect of Microchannel Geometry on High-Pressure Dispersion and Emulsification. *Chem. Eng. Technol.* **2011**, *34*, 335−343.
(28) Finke, J.; Schur, J.; Richter, C.; Gothsch, T.; Kwade, A.; Büttgenbach, S.; Müller-Goymann, C. The influence of customized geometries and process parameters on nanoemulsion and solid lipid nanoparticle production in microsystems. *Chem. Eng. J.* **2012**, *209*, 126−137.
(29) Donsì, F.; Sessa, M.; Ferrari, G. Effect of Emulsifier Type and Disruption Chamber Geometry on the Fabrication of Food Nanoemulsions by High Pressure Homogenization. *Ind. Eng. Chem. Res.* **2012**, *51*, 7606−7618.
(30) Raikar, N. B.; Bhatia, S. R.; Malone, M. F.; Henson, M. A. Experimental studies and population balance equation models for breakage prediction of emulsion drop size distributions. *Chem. Eng. Sci.* **2009**, *64*, 2433−2447.
(31) Håkansson, A.; Trägårdh, C.; Bergenståhl, B. Dynamic simulation of emulsion formation in a high pressure homogenizer. *Chem. Eng. Sci.* **2009**, *64*, 2915−2925.
(32) Taylor, G. I. The Viscosity of a Fluid Containing Small Drops of Another Fluid. *Proc. R. Soc. London, Ser. A* **1932**, *138*, 41−48.
(33) Taylor, G. The formation of emulsions in definable fields of flow. *Proc. R. Soc. London, Ser. A* **1934**, *146*, 501−523.
(34) Hinze, J. O. Fundamentals of the hydrodynamic mechanism of splitting in dispersion processes. *AIChE J.* **1955**, *1*, 289−295.
(35) Seekkuarachchi, I. N.; Tanaka, K.; Kumazawa, H. Formation and Charaterization of Submicrometer Oil-in-Water (O/W) Emulsions, Using High-Energy Emulsification. *Ind. Eng. Chem. Res.* **2006**, *45*, 372−390.
(36) Wooster, T. J.; Golding, M.; Sanguansri, P. Impact of oil type on nanoemulsion formation and Ostwald ripening stability. *Langmuir* **2008**, *24*, 12758−65.
(37) Shinnar, R. On the behaviour of liquid dispersions in mixing vessels. *J. Fluid Mech.* **1961**, *10*, 259−275.
(38) Boxall, J. A.; Koh, C. A.; Sloan, E. D.; Sum, A. K.; Wu, D. T. Droplet size scaling of water-in-oil emulsions under turbulent flow. *Langmuir* **2012**, *28*, 104−10.
(39) Nazarzadeh, E.; Sajjadi, S. Viscosity effects in miniemulsification via ultrasound. *AIChE J.* **2010**, *56*, 2751−2755.
(40) Coulaloglou, C.; Tavlarides, L. Description of interaction processes in agitated liquid-liquid dispersions. *Chem. Eng. Sci.* **1977**, *32*, 1289−1297.
(41) Marchisio, D. L.; Vigil, R. D.; Fox, R. O. Quadrature method of moments for aggregation-breakage processes. *J. Colloid Interface Sci.* **2003**, *258*, 322−334.
(42) Luo, H.; Svendsen, H. F. Theoretical model for drop and bubble breakup in turbulent dispersions. *AIChE J.* **1996**, *42*, 1225−1233.
(43) Narsimhan, G.; Gupta, J.; Ramkrishna, D. A model for transitional breakage probability of droplets in agitated lean liquid-liquid dispersions. *Chem. Eng. Sci.* **1979**, *34*, 257−265.
(44) Ramkrishna, D.; Mahoney, A. W. Population balance modeling. Promise for the future. *Chem. Eng. Sci.* **2002**, *57*, 595−606.
(45) Qian, C.; McClements, D. J. Formation of nanoemulsions stabilized by model food-grade emulsifiers using high-pressure homogenization: Factors affecting particle size. *Food Hydrocolloids* **2011**, *25*, 1000−1008.
(46) Tcholakova, S.; Vankova, N.; Denkov, N. D.; Danner, T. Emulsification in turbulent flow:: 3. Daughter drop-size distribution. *J. Colloid Interface Sci.* **2007**, *310*, 570−589.

DOI: 10.1021/acs.langmuir.6b01862
Langmuir 2016, 32, 11551−11559